



Disentangling the Hydrological and Hydraulic Controls on Streamflow Variability in E3SM V2 – A Case Study in the Pantanal Region

Donghui Xu^{1*}, Gautam Bisht¹, Zeli Tan¹, Chang Liao¹, Tian Zhou¹, Hong-Yi Li², L. Ruby Leung¹

¹Atmospheric Sciences and Global Change Division, Pacific Northwest National Laboratory, Richland, WA, USA

²Department of Civil and Environmental Engineering, University of Houston, Houston, Texas, USA

Correspondence to: Donghui Xu (donghui.xu@pnnl.gov)

Abstract. Streamflow variability plays a crucial role in shaping the dynamics and sustainability of Earth's ecosystems, which can be simulated and projected by river routing model coupled with land surface model. However, the simulation of streamflow at large scales is subject to considerable uncertainties, primarily arising from two related processes: runoff generation (hydrological process) and river routing (hydraulic process). While both processes have impacts on streamflow variability, previous studies only calibrated one of the two processes to reduce biases in the simulated streamflow. Calibration focusing only on one process can result in unrealistic parameter values to compensate for the bias resulted from the other process, thus other water related variables remain poorly simulated. In this study, we performed several experiments with the land and river components of Energy Exascale Earth System Model (E3SM) over the Pantanal region to disentangle the hydrological and hydraulic controls on streamflow variability in coupled land-river simulation. Our results show that the generation of subsurface runoff is the most important factor for streamflow variability contributed by runoff generation process, while floodplain storage effect and main channel roughness have significant impacts on streamflow variability through the river routing process. We further propose a two-step procedure to robustly calibrate the two processes together. The impacts of runoff generation and river routing on streamflow are appropriately addressed with the two-step calibration, which may be adopted by Land Surface Model and Earth System Model developers to improve modelling of streamflow.

1 Introduction

Streamflow represents a critical component in the water cycle and an essential freshwater resource to humanity. As the response of the land surface to atmosphere forcings (i.e., precipitation, temperature, radiation, etc.), streamflow exhibits strong seasonality and annual variability that varies regionally (Dettinger and Diaz, 2000). It is vital to understand streamflow variation for any region, since it has critical impacts on water management (Dobriyal et al., 2017), irrigation (Slater and Villarini, 2017), flooding control (Xu et al., 2021), and ecosystem services (Knight et al., 2014). As the hydrological cycle is



30 intensified by global warming, streamflow characteristics (Xu et al., 2021; Milly et al., 2005; Gudmundsson et al., 2021; Hirabayashi et al., 2013; Bloschl et al., 2017) such as magnitude, seasonality, and frequency may also be modulated. Robust predictions of streamflow variation are crucial for adapting to the consequences of global warming in the future.

Land surface models (LSMs) coupled with river transport models (RTMs) and fully coupled Earth system models (ESMs) have been used to predict the variability of streamflow at large scales to assess water availability and flood risk (Hirabayashi et al., 2013; Milly et al., 2002; Schewe et al., 2014). However, it remains challenging for the current generation of large-scale models to capture the streamflow seasonality accurately (Xu et al., 2021; Zhang et al., 2016). In addition, the sensitivity of streamflow to climate change is not well represented in existing model simulations (Lehner et al., 2019; Xu et al., 2022a), resulting in inevitable low confidence in the future projections. Although multiple downscaling approaches that use observations as constraints have been applied to reduce model biases in their future projections (Knutti et al., 2017; Lehner et al., 2019; Tebaldi et al., 2005; Yang et al., 2017), the corresponding uncertainty may not be constrained appropriately due to the resolution mismatch between observation and simulations (Xu et al., 2019; Smith et al., 2009). Therefore, it is necessary to improve the model performance before any reliable conclusions on future projections can be made. The most common way of improving the performance is to calibrate model parameters, which contribute an important source of model uncertainty (Ricciuto et al., 2018; Qian et al., 2018; Qian et al., 2016; Cheng et al., 2021).

45 The uncertainties of simulated streamflow variability stem from two major natural processes: runoff generation and river routing. Specifically, runoff is first generated in the LSMs (or land component in ESM), whose variability is controlled by hydrological processes, such as infiltration, evapotranspiration, wetland inundation, and soil water dynamics. TOPMODEL (Beven and Kirkby, 1979; Niu et al., 2005), and Variable Infiltration Capacity (VIC; Liang et al., 1994) are the two most widely used runoff generation parameterizations (Sheng et al., 2017). It has been demonstrated that calibrating relevant parameters in LSMs leads to improved performance in the simulated runoff at site level (Denager et al., 2022), at the watershed scale (Hou et al., 2012; Huang et al., 2013; Liao and Zhuang, 2017), continent scale (Troy et al., 2008; Yang et al., 2019), and global scale (Yang et al., 2021; Xu et al., 2022a). The simulated runoff is then routed as streamflow to the outlet through the river network in RTMs (or river component in ESM). Global RTMs routinely solve kinematic or diffusion-wave approximations of 1D Saint-Venant equations to achieve computational efficiency (Shaad, 2018). Although the physical process of fluid motion is simplified, the performance of river routing is acceptable in large basins at the monthly time steps, particularly after considering water management effects (Li et al., 2015; Yamazaki et al., 2011; Zhou et al., 2020). Topographic characteristics and channel geometry parameters, which can be derived from finer-resolution topography data, have significant impacts on the simulated hydrograph (Wu et al., 2011; Yamazaki et al., 2009). However, those parameters still need to be calibrated to improve routing process description (Hirpa et al., 2018; Jiang et al., 2021; Xu et al., 2022b) due to resolution mismatch between model and river networks in the real world (Liao et al., 2022).

Although parameters from both the runoff generation (i.e., hydrological control) and river routing processes (i.e., hydraulic control) significantly influence the streamflow variability, previous studies only focus on one of the processes for



calibration (Hirpa et al., 2018; Huang et al., 2013; Yang et al., 2019; Yang et al., 2021; Mao et al., 2019; Xu et al., 2022b). Calibrating only one process can result in unrealistic parameters to compensate for bias resulted from the other process. 65 Furthermore, a comprehensive calibration needs to consider both processes together, requiring a better understanding of the separate controls from these two processes on streamflow variability. In this study, we aim to disentangle the hydrological and hydraulic controls on the streamflow variability in the coupled land-river configuration of the Energy Exascale Earth System Model (E3SM; Golaz et al., 2019), a fully coupled ESM. The Pantanal region is selected as our study domain because it is challenging for coupled land-river model to simulate its streamflow variability accurately (Schrapffer et al., 2020; Bravo et al., 70 2012). Specifically, the streamflow seasonality of the Pantanal region is much delayed relative to the precipitation seasonality (e.g., ~5 months). Schrapffer et al. (2020) found the floodplain plain storage effects explain the 5 months delay, but the impacts of hydrological processes were not investigated, making it unclear how the delay is attributed to runoff generation and river routing processes. The significant delay in streamflow seasonality makes Pantanal region an ideal test domain to investigate the separate impacts of hydrological and hydraulic processes on streamflow variability in models. This is because a general watershed has streamflow seasonality closer to precipitation seasonality, hence the uncertainty from atmosphere forcings can be more significant than that from parameterizations. In Sec 2, we briefly introduce the model configuration, study domain, experiment designs, and calibration procedure. We also introduce a modified wetland inundation scheme to improve the representation of wetland inundation process in our model. The results of experimental simulations are first presented in Sec 3, followed by validation of our two-step calibration results against multiple reference datasets. Sec 4 concludes the study.

80 **2 Methods**

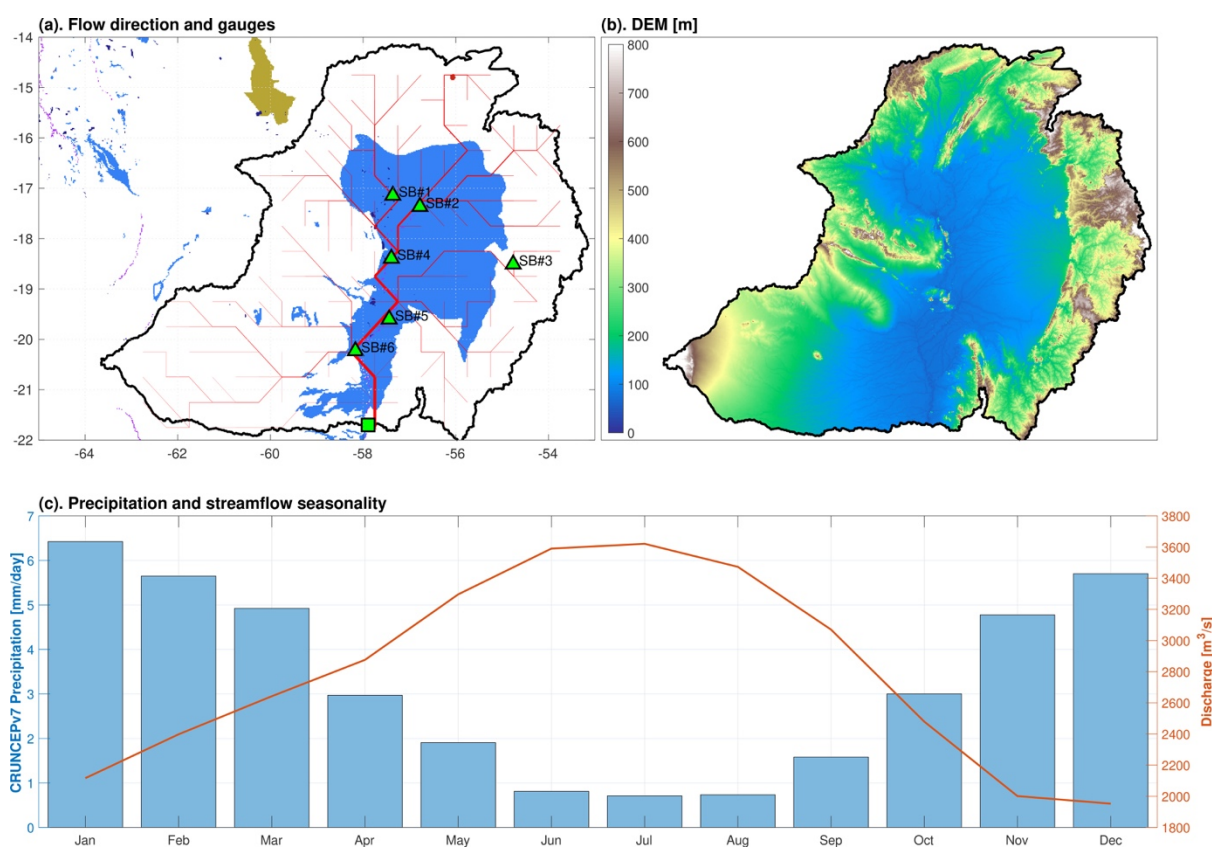
2.1 Model description

In this study, we ran the E3SM Land Model (ELM) coupled with MOSART, the river component of E3SM, to investigate the control factors of streamflow variability in coupled land-river model. ELM was developed based on Community Land Model 4.5 (CLM4.5; Oleson et al., 2013), and the same parameterizations of canopy water, snow, runoff generation, and 85 soil water dynamics were used. MOSART is a physically based river routing model that has been coupled with ELM to simulate water transport, including hillslope routing, subnetwork routing, and main channel routing (Li et al., 2013). Luo et al. (2017) coupled a macro floodplain inundation scheme with MOSART to simulate riverine inundation process, which is a necessary process to improve the river model performance (Yamazaki et al., 2011; Decharme et al., 2012; Schrapffer et al., 2020). Water management also plays a crucial role in shaping the streamflow variability (Voisin et al., 2013), but it doesn't have a significant 90 impacts in Pantanal region (Jardim et al., 2020).

2.2 Study domain



95 The Pantanal region, located in the upper Paraguay river basin (Figure 1a), is the world’s largest wetland (Ivory et al., 2019; Erwin, 2009). The wetland region may be formed due to the low-lying surface elevation, surrounded by mountains (Figure 1b). The precipitation of this region has strong seasonality, high in January and February and low during June, July, and August (Figure 1c). However, the streamflow shows a shift of about five months in the seasonality compared to precipitation (Figure 1c). We hypothesize the significant delayed response of streamflow to precipitation attributes to both hydrological and hydraulic processes.



100 **Figure 1.** (a). Study domain of upper Paraguay basin. The red line shows the river network, and the green square denotes the streamflow outlet (i.e., station Porto Murтинho) used in this study. The green triangles are the sub-basin (SB) gauges that used for evaluation. The blue area represents floodplain according to Global Lakes and Wetlands Database of Lehner and Döll (2004); (b). DEM at 90m resolution of Hydrological Data and Maps Based on Shuttle Elevation Derivatives at Multiple Scales (HydroSHEDS; Lehner et al., 2008); and (c). Precipitation seasonality derived from CRUNCEPv7 (bar plot relies on left Y-Axis) and observed streamflow seasonality from the outlet of upper Paraguay basin (red solid line relies on right Y-Axis) during 1979-2009.

105



2.3 Model setup

We ran one-way coupled ELM-MOSART (i.e., runoff simulated by ELM is send to MOSART for routing) simulations at a spatial resolution of $0.5^\circ \times 0.5^\circ$ for 1979-2009. The simulations were forced by CRUNCEPv7 atmosphere forcing in this study since it was found to be most accurate over the Pantanal region (Schrapffer et al., 2020). CRUNCEPv7 is a 6-hourly $0.5^\circ \times 0.5^\circ$ global forcing dataset that was generated based on Climatic Research Unit Time-Series Version 3.24 (CRU TS v3.24; Harris et al., 2014) and NCEP reanalysis (Kalnay et al., 1996). The time step for ELM and MOSART is 30 [min] and 60 [min], respectively, with a coupling frequency of 180 [min].

We performed 9 experiments as listed in Table 1 to investigate the sensitivity of streamflow to different processes. The first experiment is the control simulation, using the default ELM surface data and parameters and the default MOSART parameters. In experiment 2, floodplain inundation was turned on to show the impact of floodplain water storage on the streamflow seasonality. Experiment 3 tested the uncertainty of river geometry, and Experiment 4 tested the uncertainty of main channel Manning coefficient (n_r). In Experiment 5, we perturb the decay factor for the subsurface runoff generation (f_{drai}), which has been identified as the most sensitive parameter for subsurface water dynamics (Huang et al., 2013; Bisht et al., 2018). In experiment 6, we aim to understand how streamflow is affected by wetland inundation process, for which f_{over} and f_c are critical parameters (See Text S1). Experiment 7 represents calibration of river routing processing, including both geometry and Manning coefficient as uncertain. Experiment 8 calibrates both subsurface and surface water dynamics processes in runoff generation process. Lastly, experiment 9 is the proposed two-step calibration with all the parameters from experiments 3-6 included (details can be found in Sec 2.5). We used the diffusion wave routing in MOSART for all the experiments to include backwater effects.

River geometry is assumed to be rectangular (Figure 1a of Luo et al. (2017)), and the main channel bankfull width (w), and depth (d) can be derived with the equations proposed by Andreadis et al. (2013):

$$w = a_w Q^{0.5}, \quad \text{Eq (1)}$$

$$d = a_d Q^{0.3}, \quad \text{Eq (2)}$$

where Q is the 2-year return period daily streamflow, which is estimated at each grid cell by aggregating daily runoff of Reach-level Flood Reanalysis dataset (GRFR; Yang et al., 2021) from the corresponding upstream area, and a_w and a_d are curve fitting parameters. Andreadis et al. (2013) found the 95% confidence intervals for a_w and a_d are [2.6, 20.2] and [0.12, 0.63], respectively. Subsurface runoff (R_{drai}) is parameterized as exponential function of f_{drai} and water table depth (z_T):

$$R_{drai} = q_{drai,max} \exp(-f_{drai} z_T), \quad \text{Eq (3)}$$

where $q_{drai,max}$ is the maximum drainage rate. A surface water storage (i.e., depression areas where excess runoff accumulates) (Ekici et al., 2019) was introduced in ELM to simulate wetlands and sub-grid water bodies, and details can be found in Text S1. A modified wetland scheme of Xu et al. (2023b) is adopted here to improve the wetland inundation simulation (see details in Text S1), and two parameters were found to be sensitive for the wetland inundation: f_{over} and f_c .



In summary, a_w , a_d , and n_r are the parameters in MOSART and experiment 2, 3, 4, and 7 are hydraulic sensitivity experiments. f_{drai} , f_{over} , and f_c are the parameters in ELM and experiment 5, 6, and 8 are hydrology sensitivity experiments.

Table 1. Simulation experiments design

#	Experiment	Inundation mode	Parameters	Objective	Number of simulations
1	Default	off	Default	Streamflow seasonality	1
2	Inundation	on	Default	Streamflow seasonality	1
3	Geometry	on	$a_w \sim U(2.6, 20.2)$ $a_d \sim U(0.12, 0.63)$	Streamflow seasonality	100
4	Manning coefficient	on	$n_r \sim U(0.01, 0.2)$	Streamflow seasonality	100
5	Subsurface runoff	on	$f_{drai} \sim U(0.1, 5)$	Streamflow seasonality	100
6	Wetland inundation	on	$f_{over} \sim U(0.1, 5)$ $\log(f_c) \sim U(1e^{-3}, 1e^{-0.155})$	Streamflow seasonality	100
7	MOSART calibration	on	a_w, a_d, n_r	Streamflow seasonality	1,000
8	ELM calibration	on	f_{drai}, f_{over}, f_c	Streamflow seasonality	1,000
9	Two-step calibration	on	$a_w, a_d, n_r, f_{drai}, f_{over}, f_c$	Multi-objectives	2,000



Multiple datasets of site observations, satellite observations, and reanalysis products were used in this study for model calibration and evaluation. The simulated streamflow was validated at monthly and annual time scales. We used monthly streamflow observation at gauge Porto Murtinho (basin outlet shown in Figure 1a) and 6 internal subbasin gauges (Figure 1a) that archived in Global Stream Indices and Metadata (GSIM; Do et al., 2018; Gudmundsson et al., 2018). The three global runoff datasets that were used to benchmark the performance of annual streamflow include Global Runoff Reconstruction (GRUN; Ghiggi et al., 2019), Linear Optimal Runoff Aggregate (LORA; Hobeichi et al., 2019), and Global Reach-level Flood Reanalysis (GRFR; Yang et al., 2021). The global surface water dynamics dataset from Global Land Analysis & Discovery (GLAD; Pickens et al., 2020) was used to validate the simulated surface water fraction (SWF), which is the sum of ELM-simulated inundation and MOSART-simulated inundation in E3SM (Xu et al., 2023b). GLAD provides global monthly, annual, and seasonal surface water and permanent water layer derived from Landsat images during 1999-2020 at $0.00025^\circ \times 0.00025^\circ$. We used seasonal GLAD and removed the permanent water to exclude the rivers and lakes from the SWF. The GLAD was upscaled to $0.5^\circ \times 0.5^\circ$ by averaging the values from all the finer resolution grid cells within the coarse model resolution grid cell to compare with the model simulations. The gridded energy flux data (FLUXCOM; Jung et al., 2019) and Global Land Evaporation Amsterdam Model version 3 (GLEAMv3; Martens et al., 2017) product were used to evaluate evapotranspiration (ET).

2.5 Calibration procedure

We propose a two-step calibration procedure in this study to appropriately resolve hydrological and hydraulic impacts on streamflow variability. In the first step, we run 1,000 simulations with runoff generation-related parameters (f_{drain} , f_{over} , and f_c) randomly sampled from the prior distributions given by experiment 8 in Table 1. A multi-objective function was proposed by Yang et al. (2019) to calibrate a land surface model, which is adopted in this study. The best parameter was calibrated in each individual grid cell to minimize the following objective function (obj) to capture SWF, baseflow index (BFI), and annual streamflow trend (Trend) simultaneously:

$$obj = w_1 \cdot \left| \log \left(\frac{SWF_{sim}}{SWF_{glad}} \right) \right| + w_2 \cdot \left| \log \left(\frac{BFI_{sim}}{BFI_{GSCD}} \right) \right| + w_3 \cdot \left| \log \left(\frac{Trend_{sim}}{Trend_{obs}} \right) \right|, \quad \text{Eq (4)}$$

where SWF_{sim} represents annual averaged simulated surface water fraction from coupled ELM-MOSART simulation, SWF_{glad} is the GLAD annual averaged surface water fraction. SWF was estimated between 1999-2009, when the simulation period overlapped with GLAD temporal availability. BFI_{sim} and BFI_{GSCD} are the baseflow index (i.e., the ratio of subsurface runoff to total runoff) from simulations and Global Streamflow Characteristics Dataset (GSCD; Beck et al., 2013), respectively. $Trend$ denotes the trend of annual runoff quantified by Sen's slope (Sen, 1968). Because there is no reliable gridded dataset of long-term runoff trend, we assumed $Trend_{obs}$ to be constant over the whole basin, and the value was derived from observed streamflow at the outlet. Due to the different bias magnitude and uncertainty pattern, the assignment of weights is subjective (Yang et al., 2019). In the second calibration step, another 1,000 simulations were performed with river routing parameters

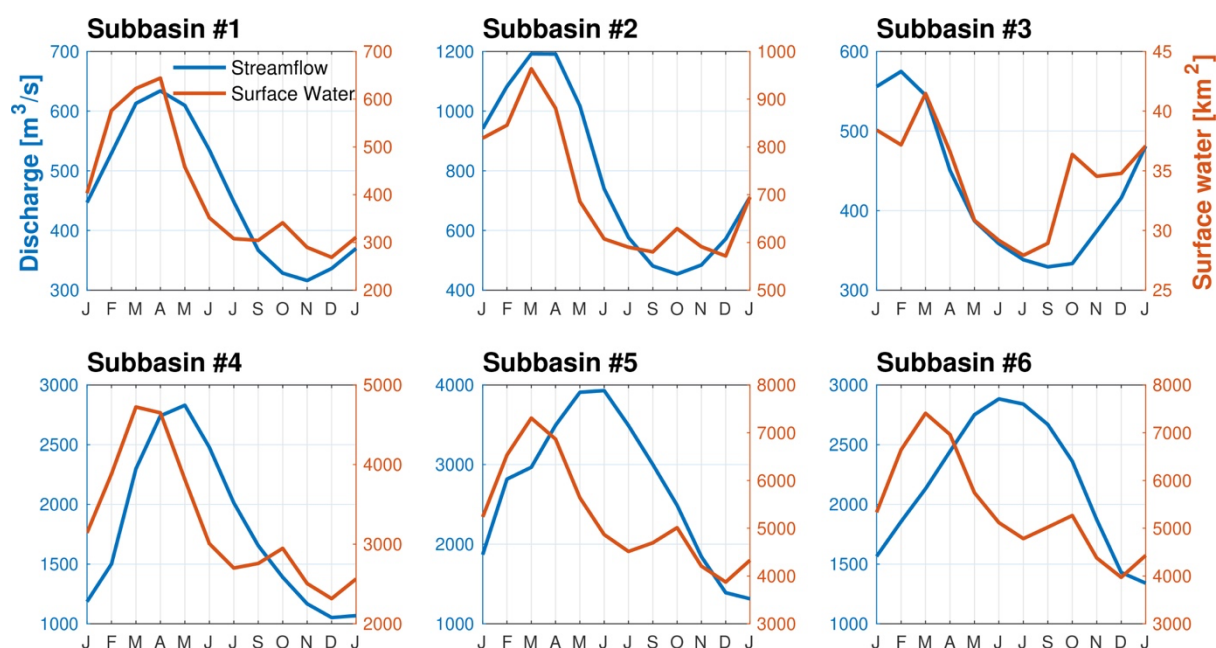


175 (a_w , a_d , and n_r) randomly sampled from the uniform distribution in Table 1 and the calibrated hydrological parameters from first step. The best a_w , a_d , and n_r were calibrated at basin level by maximizing the correlation coefficient between monthly simulated and observed streamflow at outlet. As suggested by Shen et al. (2022), we used all the streamflow observation for calibration without splitting to validation period. We further validate the calibrated model at six internal sub-basin gauges (Figure 1a), which are not used during the calibration process.

3 Results and discussion

3.1 Streamflow variability in Pantanal region

180 Figure 2 illustrates the observed streamflow seasonality from 6 selected sub-basins in Pantanal region, with the streamflow peaks shift from March in the headwater (sub-basin #1, #2, and #3) to June in downstream of the river (sub-basin #6). Streamflow variability reflects the combined effects of routing surface runoff and subsurface runoff. Surface runoff is closely related to the surface water dynamics, which is controlled by the hydraulic factor, such as floodplain inundation process. However, the surface water dynamics has a much earlier seasonality (i.e., peak in March) than the streamflow at the downstream gauges (Subbasin #4, #5, and #6). The differences in the seasonality between surface water dynamics and outlet streamflow imply the significant contribution of subsurface runoff to the streamflow variability. The subsurface runoff generation is hydrological process, simulated by land surface model (e.g., ELM). Therefore, both hydrological and hydraulic processes have impacts on the significant shift in the seasonality between precipitation and streamflow in Pantanal region.

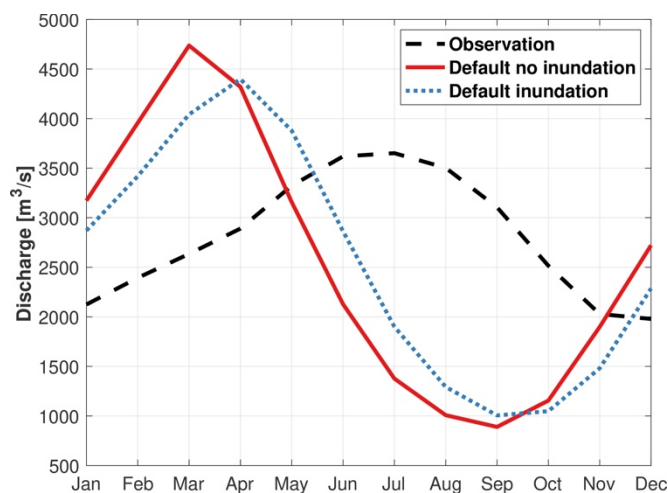




190 **Figure 2.** Streamflow seasonality derived from GSIM observation during 1979-2009 (blue solid line) and seasonality of surface water dynamic from GLAD dataset (red solid line) at sub-basins in Pantanal region.

3.2 Impacts of MOSART on streamflow variability

The coupled ELM-MOSART simulation with the default configuration and parameters fails to capture the streamflow seasonality over the Pantanal region. Specifically, the default simulation shows streamflow peaks around March, which is much earlier than the observed streamflow peaks in July (Figure 3). Previous studies found that the late responses of streamflow peaks to precipitation are caused by the storage effects of floodplain (Schrapffer et al., 2020). However, in our inundation experiment, turning on the inundation mode only delays the streamflow seasonality by one month compared to the default configuration, which still cannot capture the observed seasonality well (Figure 3). This discrepancy suggests significant uncertainties exist in other river routing or runoff generation-related parameters. For example, our geometry experiment demonstrates that smaller a_w and a_d lead to a higher model performance of capturing streamflow seasonality, such as a higher correlation coefficient of monthly streamflow between simulation and observation (Figure 4a). Smaller a_w and a_d (i.e., smaller cross-section area) correspond less channel capacity, implying that more water will inundate on floodplain during flooding period, therefore, the peak streamflow is delayed to a later time. Although the streamflow seasonality is improved by reducing channel cross-section area, it results in smaller temporal variations in monthly streamflow, such as the ratio of standard deviation (rSD) between simulation and observation being less than 0.85. The smaller rSD indicates the regulation of the floodplain is magnified; therefore, it is not reasonable to accept such small channel geometry.



210 **Figure 3.** Simulated streamflow seasonality of default simulation (experiment 1 in Table 1), and default simulation with inundation mode (experiment 2 in Table 1). The seasonality is derived from 1979 to 2009.



The Manning coefficient of the main channel affects the streamflow seasonality through its impacts on flow velocity. In our experiment of the Manning coefficient, increasing the channel Manning coefficient will at most shift the occurrence of peak streamflow to June (Figure 4b), while the corresponding value ($nr \geq 0.16$) is much higher than the generally used main channel Manning coefficient in global river transport models (e.g., 0.03-0.06; Yamazaki et al., 2011; Li et al., 2013; Decharme et al., 2012). Larger Manning coefficient means slower flow velocity along the river direction, then the water will accumulate in the channel and inundate the floodplain when it exceeds the channel capacity. Notably, such high main channel Manning coefficients lead to an unrealistic flatter hydrograph with $rSD < 0.7$. Using Manning coefficient at around 0.1 reproduces the monthly variability best (e.g., $rSD = 1$), which is still higher than the typical value, but such a range may be reasonable in this region because of the vegetated surface and complex river network (i.e., meandering) according to Chow (1959). The subnetwork and hillslope Manning coefficients in MOSART are not included in our experiments because they have negligible impacts on the shape of the hydrograph (Figure S3).

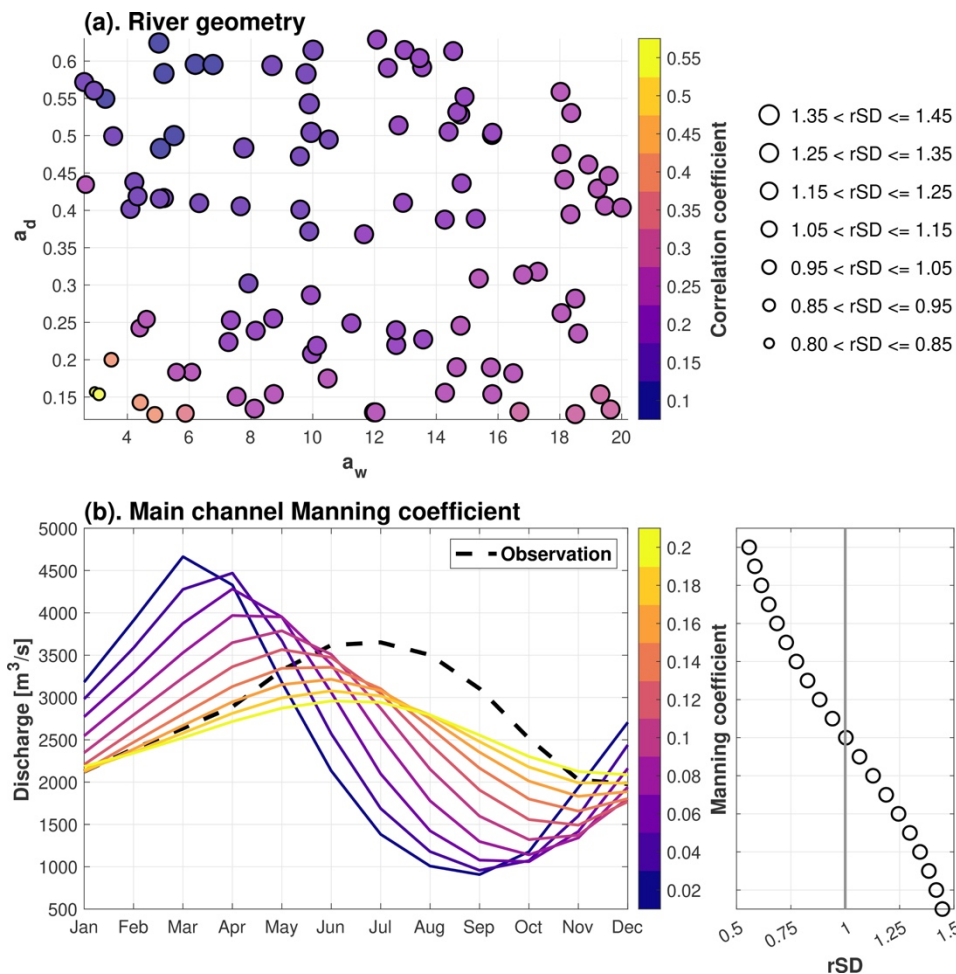
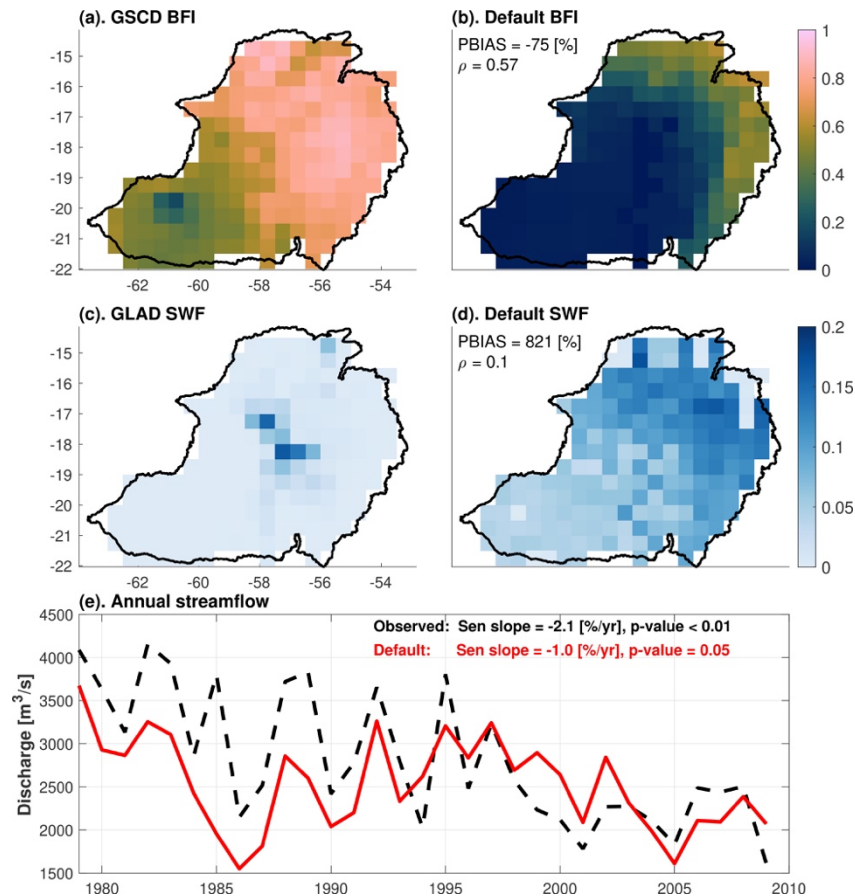




Figure 4. Sensitivity of streamflow seasonality and variability to (a). river geometry, and (b) main channel Manning
225 coefficient. In subplot (a), a_w and a_d are the parameters for river width and depth, respectively (Eq (1) and Eq (2)), and the
correlation coefficient between the simulated streamflow and observed streamflow at monthly scale is used to indicate the
model performance of simulating streamflow seasonality. The scatter size is proportional to the ratio of standard deviation
(rSD) between the simulated streamflow and observation. The black dashed line in subplot (b) represents the averaged
streamflow seasonality derived from observation. And the scatter on the right shows the relationship between the main channel
230 manning coefficient (Y-axis) and rSD (X-axis).

Although calibrating channel geometry and Manning coefficient improves the performance of the coupled ELM-
MOSART model in simulating streamflow, there exist some discrepancies in the streamflow seasonality and variation between
simulation and observation. Floodplain effects cannot completely explain the streamflow seasonality in the Pantanal region.
235 Additionally, other variables in the water cycle remain highly biased, which cannot be fixed by calibrating river routing-related
parameters. First, the simulated BFI averaged over the basin is about 0.15, which significantly underestimates the values (e.g.,
0.69) estimated by Global Streamflow Characteristics Dataset (GSCD; Beck et al., 2013) (Figure 5a and b). Second, the surface
water dynamics is poorly simulated with a low spatial correlation coefficient (0.03) and high percentage bias (715%) as
compared to GLAD (Figure 5c and d). Third, the Pantanal region has become drier in the past several decades (Libonati et al.,
240 2020), which can be detected from the observed annual streamflow time series (Figure 5e). While the model is able to capture
the drier trend of annual streamflow during the simulation period (negative Sen's slope with p-value = 0.05), the magnitude of
the decreasing trend is underestimated (Figure 5e). The above discrepancies can be reduced by calibrating the runoff generation
related processes (e.g., hydrological control) because river routing process only impact the shape of the hydrograph.



245 **Figure 5.** Performance of ELM-MOSART with default configuration. (a). Base flow index (BFI) from GSCD BFI3; (b).
simulated BFI with default parameter; (c). surface water fraction (SWF) from GLAD; (d) simulated SWF (floodplain
inundation + wetland inundation) with default parameter; (e). annual streamflow time series of observation (black dashed line)
and default simulation (red solid line) at basin outlet.

250 3.3 Impacts of ELM on streamflow variability

Subsurface runoff experiment demonstrates subsurface runoff generation process has a critical control on the
streamflow seasonality as well (Figure 6). It is shown in Figure 6a that the simulated streamflow tends to peak later as f_{drain}
decreases. Decrease of f_{drain} means the subsurface storage capacity increases (Huang et al., 2013), therefore, leading to a
higher base flow index (Figure 6b). This explains the response of total runoff to rainfall is delayed when smaller f_{drain} was
255 used due to the slower mechanism of subsurface runoff (Vivoni et al., 2007). Furthermore, smaller f_{drain} leads to increased
annual streamflow magnitude but reduced monthly streamflow variability (Figure 6c). We acknowledge unrealistic high



streamflow (e.g., mean > 5,000 [$\frac{m^3}{s}$]) with minimal month-to-month variability (e.g., rSD < 0.4) are found in the simulations when f_{drain} is close to 0.1; thus, a more reasonable lower bound of f_{drain} 's prior should be modified to a larger value (e.g., 0.25). Moreover, the trend of annual simulated streamflow can be affected by f_{drain} , though all the simulations tend to
 260 underestimate the trend detected in the observation. The decreasing trend is more significant and closer to the observed trend when f_{drain} decreases (Figure 6d), except two problematic simulations with very small f_{drain} .

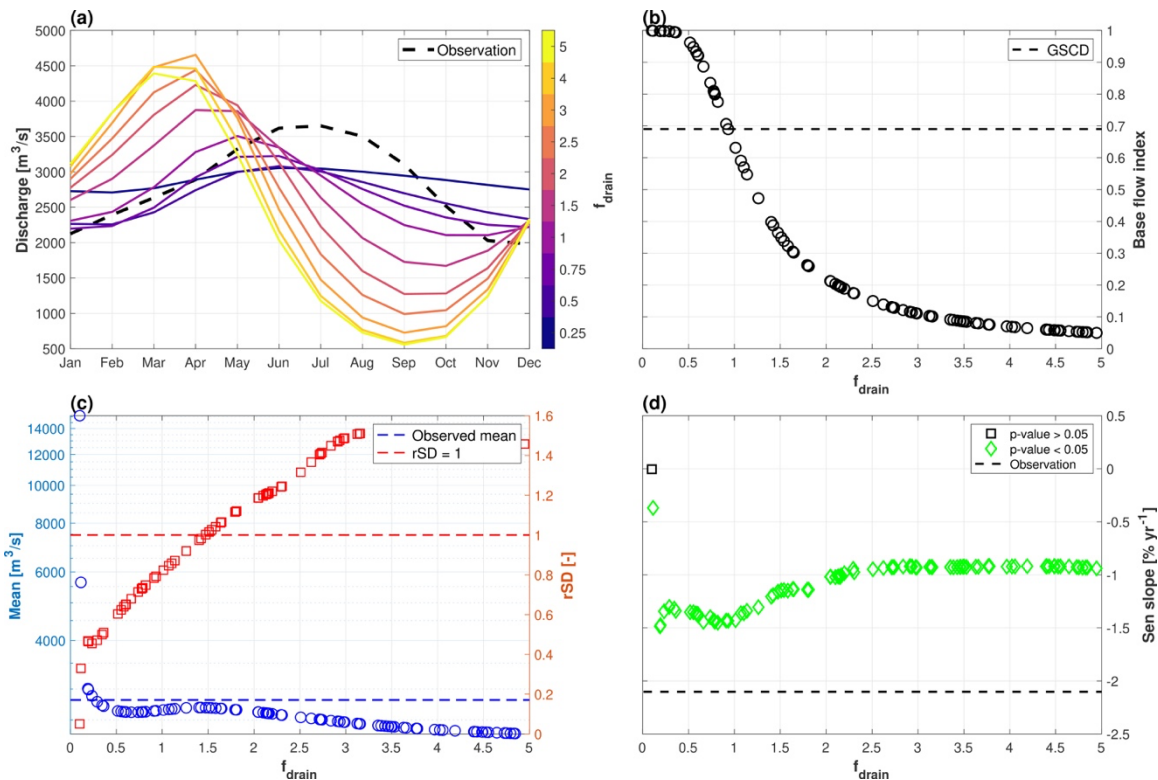
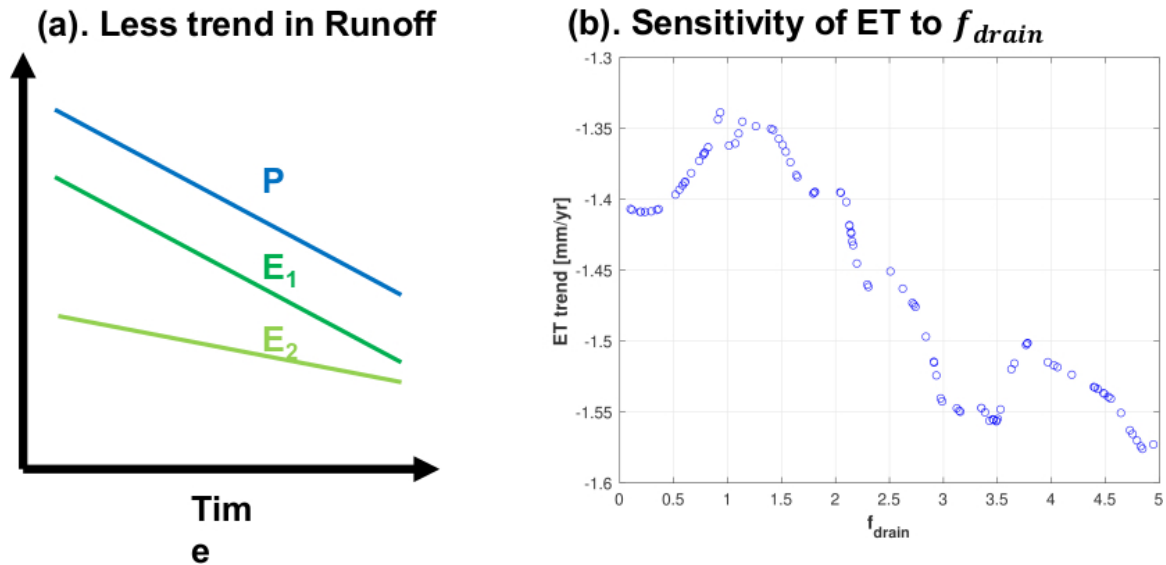


Figure 6. Sensitivity of (a). Streamflow seasonality; (b). Base flow index; (c). Annual streamflow mean and rSD; and (d).
 annual streamflow trend to f_{drain} . rSD denotes the ratio of monthly standard deviation between simulation and observation.
 265 Note, the Sen's slope is normalized by the annual averaged streamflow.

The sensitivity of annual runoff trend (i.e., annual streamflow trend) to f_{drain} results from the impacts of f_{drain} on ET processes. As a conceptual example, the runoff will not have trend in time if precipitation and ET have similar decreasing trend (e.g., P and E_1 in Figure 7a). Runoff will show a trend in time when the changing rate of ET is different from precipitation
 270 (e.g., P and E_2 in Figure 7a). The experiment of f_{drain} shows that the ET is less sensitive to precipitation decreases with smaller f_{drain} (Figure 7b), thus leading to a larger decreasing trend in annual runoff (light green line in Figure 7a). Based on above analyses, it is reasonable to argue that a good selection of f_{drain} in this region should be smaller than the default value

(i.e., 2.5), which will yield later streamflow seasonality and better estimates of base flow index, monthly variability, and annual trend compared to reference data or observation.

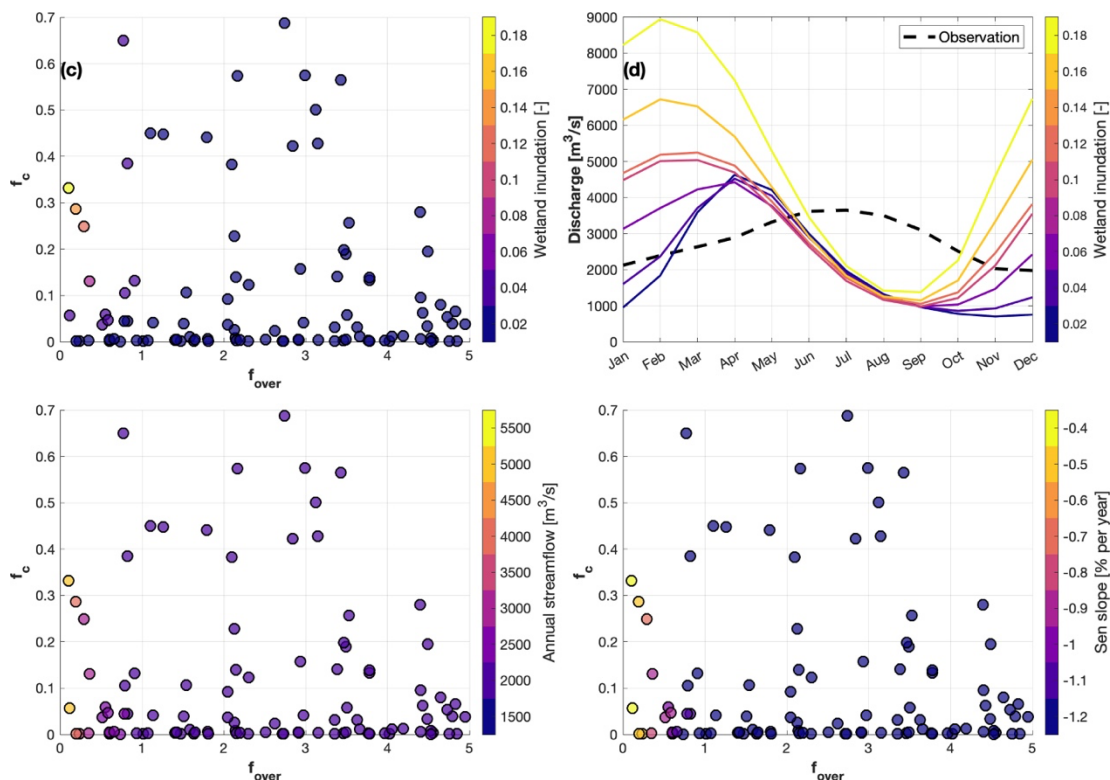


275

Figure 7. (a) Conceptual plot of annual precipitation (P) and annual evapotranspiration (ET) with different trend (E₁ and E₂). Subplot (b) shows the sensitivity of annual ET trend to f_{drain} .

Parameters f_{over} and f_c control the streamflow variability through wetland inundation process based on our wetland
inundation experiment (Figure 8a) and previous study (Xu et al., 2023b). Wetland inundation is only sensitive to f_c when f_{over}
is smaller than 0.5, as small f_{over} leads to a higher saturated fraction, at which infiltration from the wetlands is constrained and
inundation occurs (Figure S2a). In contrast to the impacts of floodplain inundation, higher wetland inundation is associated
with earlier streamflow peaks (Figure 8b). This is because high wetland inundation is caused by precipitation when the
saturation fraction is high (e.g., lower f_{over}), consequently, a larger fraction of precipitation converts to surface runoff. Hence,
the streamflow seasonality is very close to precipitation seasonality when high wetland inundation is simulated since surface
runoff responds quickly to precipitation. The annual streamflow magnitude and trend are also sensitive to the wetland
inundation process (Figure 8c and d), especially when parameter f_{over} falls in the lower range (e.g., less than 1.5). Specifically,
the annual streamflow magnitude increases, and the trend become less negative as f_{over} decreases.

285



290 **Figure 8.** Subplot (a) sensitivity of wetland inundation to f_c and f_{over} . Subplot (b) impacts of wetland inundation on streamflow seasonality. Sensitivity of (c). annual streamflow; and (d). annual streamflow trend to f_c and f_{over} . Note, the Sen's slope is normalized by the annual averaged streamflow.

3.4 Single process calibration

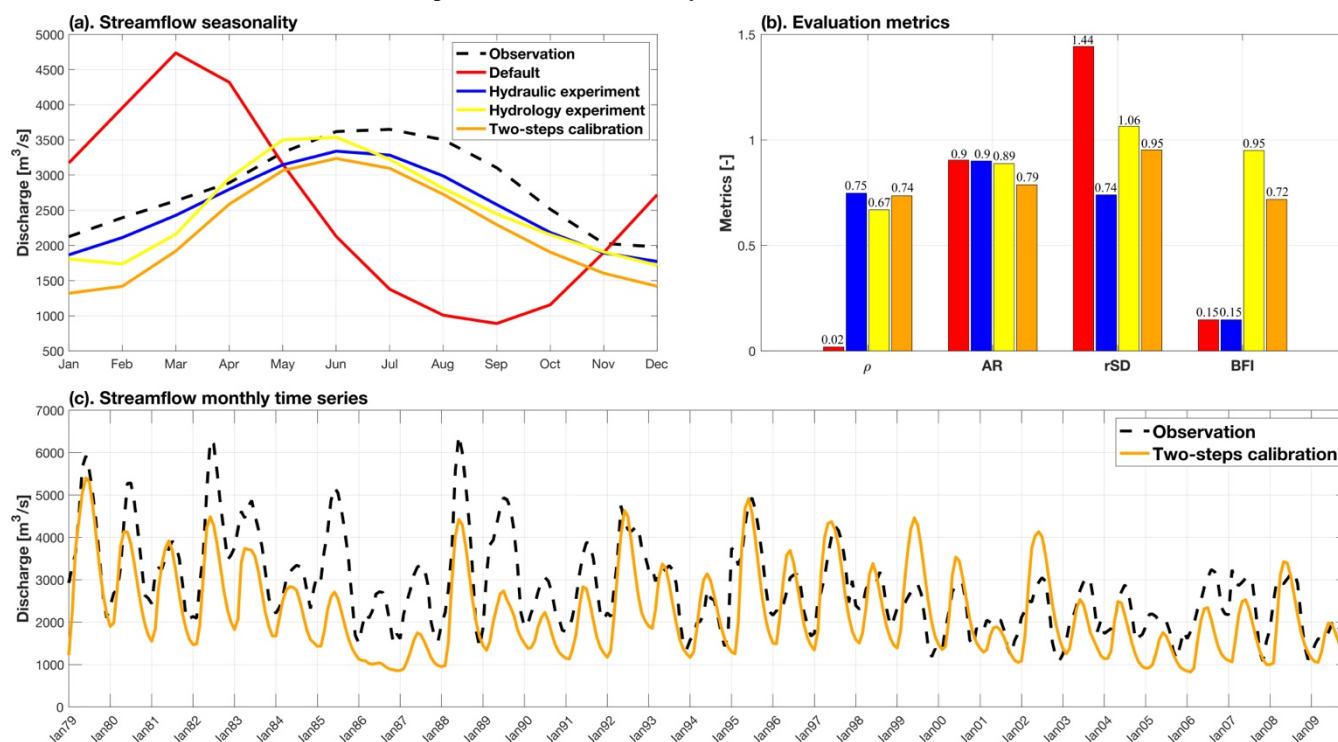
295 We further conducted two independent calibrations for either the river routing process in MOSART and the runoff generation process in ELM using experiments 7 and 8 (Table 1), respectively. Specifically, the objectives of both independent calibrations are to maximize the correlation coefficient between the simulated and observed streamflow time series. Both calibrations can improve the streamflow seasonality significantly as compared to the default configuration, with correlation coefficient increased from 0.02 to 0.75 and 0.67, respectively (Figure 9a and b). The long-term averaged annual streamflow remains similar in the default configuration and two calibrations, with all underestimating the observation by about 10%.

300 However, the temporal variations of simulated streamflow time series in the two calibrations show divergent bias patterns, with MOSART calibration resulting in a smaller standard deviation (e.g., $rSD = 0.74$), while ELM calibration leading to a slightly higher standard deviation (e.g., $rSD = 1.06$) (Figure 9b).

Individual MOSART calibration can lead to a very high Manning coefficient (e.g., $nr = 0.17$) and a smaller cross-section of the main channel to capture the streamflow seasonality. Consequently, the flow velocity is slower, and more river



305 water inundates the floodplain due to backwater effects, which results in a significant underestimation in the temporal variation
of simulated streamflow (Figure 9b). The individual ELM calibration leads to an unreasonably higher baseflow index (Figure
9b), implying the subsurface and surface water dynamics are not well represented. Overall, only calibrating the parameters
related to one process results in unrealistic parameter values to compensate the bias from the other process. Therefore, the
impacts of both runoff generation and river routing processes on streamflow must be considered together in calibrating the
310 streamflow simulation to ensure all the processes of the water cycle are well calibrated.



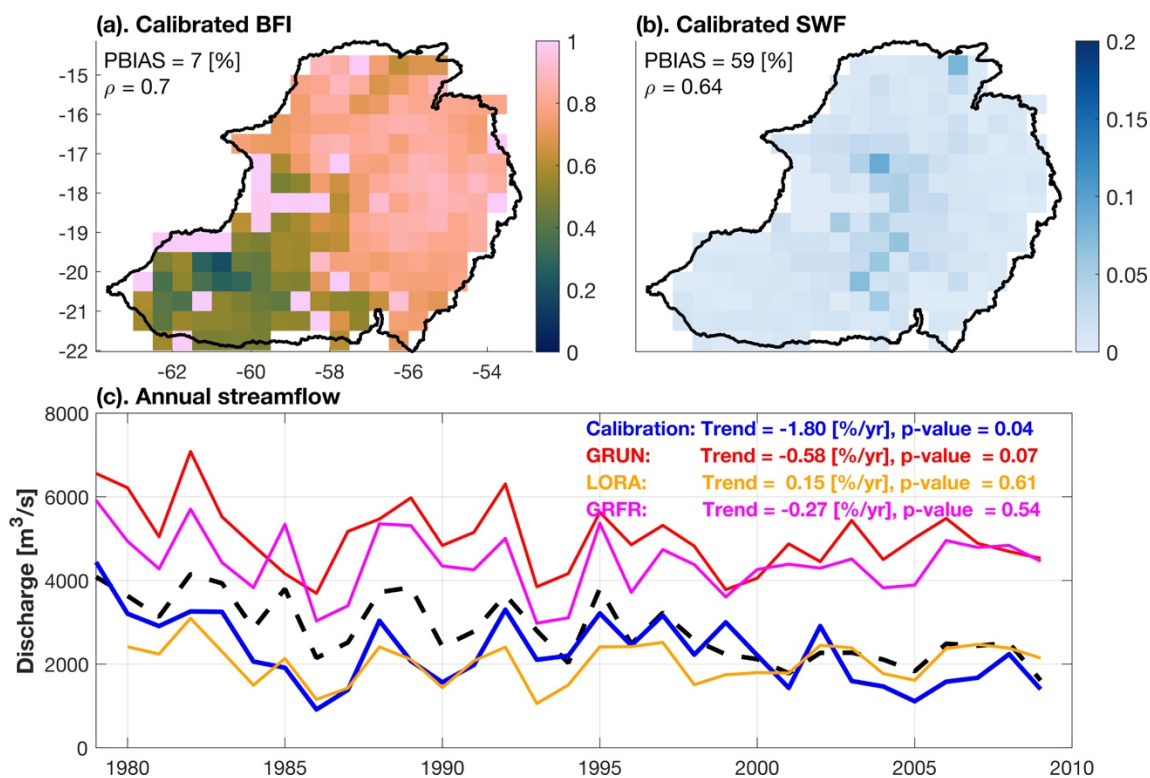
315 **Figure 9.** Comparison of hydraulic, hydrology, and two-step calibration with default configuration. Subplot (a) shows the seasonality from simulation period, and subplot (b) denotes the correlation coefficient (ρ), annual streamflow ratio (AR), ratio of standard deviation between simulation to observation (rSD), and baseflow index (BFI). Subplot (c) presents the monthly time series of simulated streamflow after two-step calibration.

3.5 Two-step calibration

We propose a two-step calibration procedure in this study (Sec 2.5) by first calibrating the runoff generation relevant parameters in ELM, and then calibrating the river routing relevant parameters in MOSART. Since it is unclear how much the streamflow delay is attributed to the runoff generation process, we use other objectives (i.e., independent of streamflow variability) in the ELM calibration (Eq (7)). It is implied from the analyses of runoff-related parameters that the runoff seasonality is related to the objectives used in Eq (7). Therefore, we assume the delay of streamflow attributed to the runoff



generation process can be addressed by minimizing Eq (4). In the multi-objective function, we found $w_1 = 0.15$, $w_2 = 0.7$, and $w_3 = 0.15$ yield the best result. The calibrated simulation shows good skill in capturing the spatial pattern of baseflow index and surface water fraction with correlation coefficients of 0.7, and 0.64, respectively, as compared to the reference data (Figure 10a and b). The absolute biases are significantly reduced as well. Moreover, the calibrated simulation shows a statistically significant decreasing trend in the annual streamflow with Sen's slope equal to -1.80 [%/yr] after normalizing with averaged annual streamflow magnitude. As a benchmark, we found other calibrated or bias-corrected runoff datasets cannot capture either the annual magnitude or annual trend (Figure 10c). The uncertainty of the annual magnitude may stem from the forcing uncertainty, while the trend bias is because model sensitivity to climate change is not well constrained. This suggests including trend as a performance metric in the objective function is necessary for calibrating ESMs, which are commonly used to project the change of water, energy, and carbon cycle under warmer climate. Although water table depth is not included in the objective function, the simulated water table depth is more consistent with the dataset of Fan et al. (2013) than the default configuration, which simulates a very shallow water table (Figure S4). The improved representation of groundwater table depth is because that the subsurface and surface runoff are correctly separated (e.g., a better simulated baseflow index).

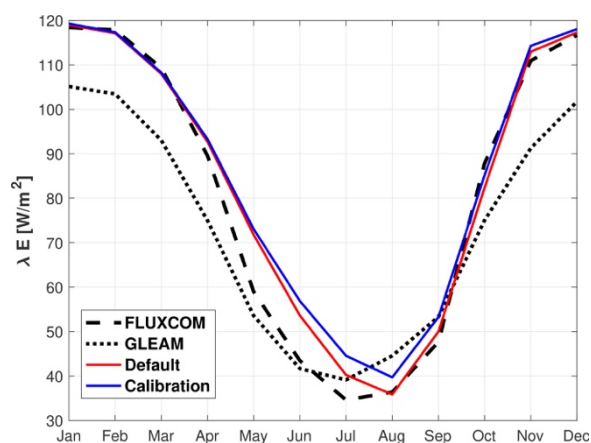


335

Figure 10. Performance of ELM-MOSART with calibrated ELM parameters for (a). Base flow index (BFI); (b). surface water fraction (SWF); and (c). annual streamflow trend. Three other runoff datasets are used to provide benchmarks for annual streamflow. The black dashed line represents the observation from the outlet.



340 With hydrology parameters determined from the first step calibration, the model shows good performance of
 simulating monthly streamflow after the second step - MOSART calibration (Figure 9c). Specifically, the correlation
 coefficient between simulation and observation at the monthly scale is 0.74, indicating the streamflow seasonality is well
 captured. Compared to the individual MOSART or ELM calibration, the two-step calibration shows better skill in both monthly
 variation (e.g., $rSD=0.95$) and baseflow index (e.g., $BFI=0.72$) (Figure 9b). However, the two-step calibration exhibits higher
 345 biases in the annual streamflow magnitude, stemming from the following reasons: 1) uncertainty of upscaled flow directions
 in MOSART because of the relatively coarse spatial resolution ($\sim 50km \times 50km$) (Liao et al., 2022). For example, the
 contributing area of the selected outlet estimated using the modeled flow direction underestimates $\sim 5\%$ of the contributing
 area that is delineated with the 1km HydroSHEDS DEM; 2) uncertainty of forcing data. Specifically, the annual averaged
 precipitation in CRUNCEPv7 is lower than the mean of multiple precipitation products (Figure S5a). There may exist biases
 350 in other forcing variables (e.g., humidity and radiation) as well, resulting in an overestimation of evapotranspiration during the
 dry period (e.g., May to July) as compared to FLUXCOM (Figure 11). For the reference ET of GLEAM dataset, the simulated
 ET is higher for all the months. In addition, Xu et al. (2023a) also reported that energy partition algorithm in current ESMS
 tends to overestimate ET. In summary, while our calibrated model underestimates streamflow magnitude, the result is
 reasonable as the negative bias is consistent with the smaller contributing area, lower precipitation forcing, and higher
 355 evapotranspiration estimates. Furthermore, CRUNCEPv7 shows a notable reduction of precipitation from January to February,
 while other precipitation products show similar precipitation volume in January and February (Figure S5b). The
 underestimation of precipitation in February further explains the slightly earlier streamflow seasonality after the two-step
 calibration.



360 **Figure 11.** Comparison of latent heat flux between simulations and references.

After the two-step calibration, both the runoff generation and river routing processes are robustly improved in E3SM over Pantanal region. Although only the observed streamflow at the basin outlet was used during the calibration, the



365 performances of simulated streamflow are improved at selected subbasin gauges compared to default configuration (Figure
 12). Specifically, the calibrated model captures the streamflow monthly variation at all the sub-basin gauges well with
 correlation coefficient larger than 0.6. While the seasonality is well captured, the calibrated model cannot reproduce the
 magnitude of streamflow well at the headwater sub-basins (Subbasin #1, #2, and #3), likely due to the uncertainty of
 precipitation in the forcing and bias of flow direction represented in MOSART (Figure S6). The relative higher uncertainties
 370 in small subbasins are expected in the context of ESM, as large-scale coupled land-river model is commonly evaluated at
 global major river basins (Yamazaki et al., 2011; Li et al., 2015; Decharme et al., 2019).

To assess the transferability and robustness of our approach, we implemented the two-step calibration procedure in a
 watershed located in a distinct climate and biome, specifically the Susquehanna River Basin. Figure S7 shows that the
 performance of simulating BFI, SWF, and streamflow seasonality are improved after the calibration with the proposed method.

375

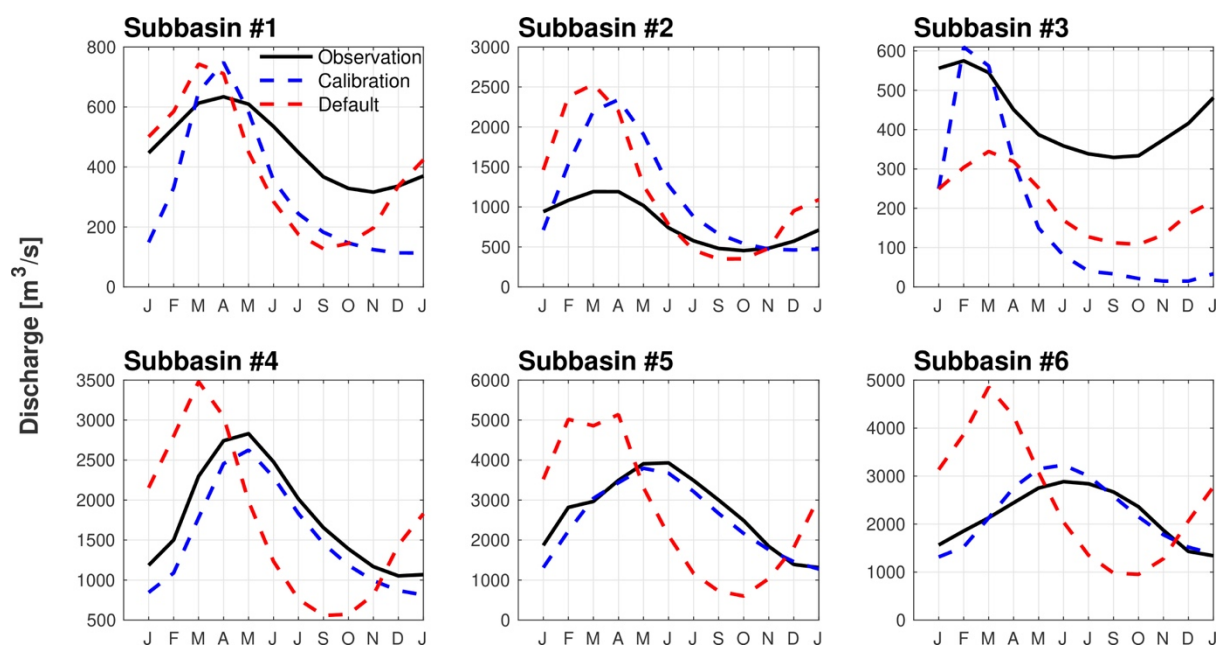


Figure 12. Simulated streamflow seasonality during 1981-2010 for the selected subbasins with default parameter values (red dashed line) and calibrated parameter values (blue dashed line). The black solid line denotes the observed streamflow seasonality.

380 4 Conclusion

In this study, we investigated the impacts of the runoff generation process and river routing process on streamflow
 variability in the coupled land and river configuration of E3SM using the Pantanal region as a case study. Previous studies
 argued that floodplain storage effects are critical in capturing streamflow seasonality in global river transport models



(Schrapffer et al., 2020; Yamazaki et al., 2011; Decharme et al., 2012), but we found that the impacts runoff generation process
385 on the streamflow variability should not be ignored. Calibrating either the runoff generation or river routing relevant parameters
can improve the performance of simulated streamflow variability, but the system as a whole is not well captured, as the
baseflow index, sensitivity of streamflow to climate change, water table depth, surface water dynamics remain highly biased.
This implies that only calibrating one of the two processes results in overfitting and problematic parameter values, i.e., the
390 impact of one process compensates for the bias resulted from the other process. Consequently, such calibration causes
unrealistic simulation of other relevant variables. Therefore, a two-step calibration procedure is proposed for large-scale
coupled land-river simulation to reconcile their impacts on streamflow variability. Specifically, the first step is to calibrate the
hydrological parameters at the grid cell level with multiple selected objectives, followed by the second step to calibrate the
river model at the basin level in terms of streamflow performance. The two-step calibration exhibits robust performance in the
water cycle simulation. The sensitivity of streamflow to climate change was improved as well in our two-step calibration,
395 suggesting the importance of including annual runoff trend in hydrological parameters calibration since trend analysis is of
particular interest in Earth system modeling. The two-step calibration method demonstrates robust performance in calibrating
E3SM coupled land-river configuration at a watershed with different climatology and biome. Future study will extend this
calibration method to E3SM at global scales. In conclusion, we suggest that both runoff generation and river routing processes
should be carefully considered together during the calibration of streamflow simulation for improving streamflow simulations
400 with coupled land-river model.

Code and Data Availability

E3SMV2 is available from E3SM-Project website: <https://github.com/E3SM-Project/E3SM> (last access: Aug 2023) under
BSD 3-clause license (<https://github.com/E3SM-Project/E3SM/blob/master/LICENSE>). The exact version of E3SM is
published at <https://github.com/donghuix/E3SM/releases/tag/v2-new-wetland-scheme> (last access: Aug 2023), and is available
405 at Zenodo: <https://doi.org/10.5281/zenodo.6982264> (Xu, 2022). Instructions of running E3SMV2 can be found at:
<https://e3sm.org/model/running-e3sm/e3sm-quick-start/> (last access: Aug 2023). Matlab version R2019b Update 4 was used
to pre-process datasets for simulations, post-process model outputs and plot results. The pre-processed datasets, Matlab pre-
and post-processing codes, and the script to run ELM-MOSART simulations are archived at Zenodo:
<https://doi.org/10.5281/zenodo.8290236> (Xu, 2023).

410 Author contribution

D.X., G.B., and Z.T. designed the study. D.X. performed the simulations and analysis and wrote the initial manuscript under
the mentorship of G.B., T.Z. and H.L. advised D.X. on MOSART model. C.L., T.Z., H.L., and R.L. investigated the results.
All authors contributed to the results discussion, review, and manuscript writing.



Competing interests

415 The authors declare that they have no conflict of interest.

Acknowledgments

This work was supported by the Earth System Model Development program area of the U.S. Department of Energy, Office of Science, Office of Biological and Environmental Research as part of the multi-program, collaborative integrated Coastal Modeling (ICoM) project. Chang Liao was supported through Next-Generation Ecosystem Experiments-Tropics, funded by
420 the U.S. Department of Energy, Office of Science, Office of Biological and Environmental Research, at Pacific Northwest National Laboratory. The Pacific Northwest National Laboratory is operated by Battelle for the U.S. Department of Energy under Contract DE-AC05-76RLO1830.

References

- 425 Andreadis, K. M., Schumann, G. J.-P., and Pavelsky, T.: A simple global river bankfull width and depth database, *Water Resour Res*, 49, 7164-7168, 10.1002/wrcr.20440, 2013.
- Beck, H. E., van Dijk, A. I. J. M., Miralles, D. G., de Jeu, R. A. M., Bruijnzeel, L. A., McVicar, T. R., and Schellekens, J.: Global patterns in base flow index and recession based on streamflow observations from 3394 catchments, *Water Resour Res*, 49, 7843-7863, <https://doi.org/10.1002/2013WR013918>, 2013.
- 430 Beven, K. J. and Kirkby, M. J.: A physically based, variable contributing area model of basin hydrology / Un modèle à base physique de zone d'appel variable de l'hydrologie du bassin versant, *Hydrological Sciences Bulletin*, 24, 43-69, 10.1080/02626667909491834, 1979.
- Bisht, G., Riley, W. J., Hammond, G. E., and Lorenzetti, D. M.: Development and evaluation of a variably saturated flow model in the global E3SM Land Model (ELM) version 1.0, *Geosci. Model Dev.*, 11, 4085-4102, 10.5194/gmd-11-4085-2018, 2018.
- 435 Bloschl, G., Hall, J., Parajka, J., Perdigo, R. A. P., Merz, B., Arheimer, B., Aronica, G. T., Bilibashi, A., Bonacci, O., Borga, M., Canjevac, I., Castellarin, A., Chirico, G. B., Claps, P., Fiala, K., Frolova, N., Gorbachova, L., Gul, A., Hannaford, J., Harrigan, S., Kireeva, M., Kiss, A., Kjeldsen, T. R., Kohnova, S., Koskela, J. J., Ledvinka, O., Macdonald, N., Mavrova-Guirguinova, M., Mediero, L., Merz, R., Molnar, P., Montanari, A., Murphy, C., Osuch, M., Ovcharuk, V., Radevski, I., Rogger, M., Salinas, J. L., Sauquet, E., Sraj, M., Szolgay, J., Viglione, A., Volpi, E., Wilson, D., Zaimi, K., and Zivkovic, N.: Changing climate shifts timing of European floods, *Science*, 357, 588-590, 10.1126/science.aan2506, 2017.
- 440 Bravo, J. M., Allasia, D., Paz, A. R., Collischonn, W., and Tucci, C. E. M.: Coupled Hydrologic-Hydraulic Modeling of the Upper Paraguay River Basin, *Journal of Hydrologic Engineering*, 17, 635-646, doi:10.1061/(ASCE)HE.1943-5584.0000494, 2012.
- Cheng, Y., Huang, M., Zhu, B., Bisht, G., Zhou, T., Liu, Y., Song, F., and He, X.: Validation of the Community Land Model Version 5 Over the Contiguous United States (CONUS) Using In Situ and Remote Sensing Data Sets, *Journal of Geophysical Research: Atmospheres*, 126, e2020JD033539, <https://doi.org/10.1029/2020JD033539>, 2021.
- 445 Chow, V. T.: *Open-channel hydraulics*, McGraw-Hill civil engineering series, 1959.
- Decharme, B., Alkama, R., Papa, F., Faroux, S., Douville, H., and Prigent, C.: Global off-line evaluation of the ISBA-TRIP flood model, *Clim Dynam*, 38, 1389-1412, 10.1007/s00382-011-1054-9, 2012.
- Decharme, B., Delire, C., Minvielle, M., Colin, J., Vergnes, J.-P., Alias, A., Saint-Martin, D., Sférian, R., Sénési, S., and Voltaire, A.: Recent Changes in the ISBA-CTrip Land Surface System for Use in the CNRM-CM6 Climate Model and in Global Off-Line Hydrological Applications, *J Adv Model Earth Sy*, 11, 1207-1252, <https://doi.org/10.1029/2018MS001545>, 2019.
- 450 Denager, T., Sonnenborg, T. O., Looms, M. C., Bogena, H., and Jensen, K. H.: Multi-objective calibration of the Community Land Model Version 5.0 using in-situ observations of water and energy fluxes and variables, *EGUsphere*, 2022, 1-41, 10.5194/egusphere-2022-406, 2022.
- Dettinger, M. D. and Diaz, H. F.: Global Characteristics of Stream Flow Seasonality and Variability, *J Hydrometeorol*, 1, 289-310, 10.1175/1525-7541(2000)001<0289:Gcosfs>2.0.Co;2, 2000.
- 455 Do, H. X., Gudmundsson, L., Leonard, M., and Westra, S.: The Global Streamflow Indices and Metadata Archive (GSIM) – Part 1: The production of a daily streamflow archive and metadata, *Earth Syst. Sci. Data*, 10, 765-785, 10.5194/essd-10-765-2018, 2018.



- Dobriyal, P., Badola, R., Tuboi, C., and Hussain, S. A.: A review of methods for monitoring streamflow for sustainable water resource management, *Applied Water Science*, 7, 2617-2628, 10.1007/s13201-016-0488-y, 2017.
- 460 Ekici, A., Lee, H., Lawrence, D. M., Swenson, S. C., and Prigent, C.: Ground subsidence effects on simulating dynamic high-latitude surface inundation under permafrost thaw using CLM5, *Geosci. Model Dev.*, 12, 5291-5300, 10.5194/gmd-12-5291-2019, 2019.
- Erwin, K. L.: Wetlands and global climate change: the role of wetland restoration in a changing world, *Wetlands Ecology and management*, 17, 71-84, 2009.
- Fan, Y., Li, H., and Miguez-Macho, G.: Global Patterns of Groundwater Table Depth, *Science*, 339, 940-943, 10.1126/science.1229881, 2013.
- 465 Ghiggi, G., Humphrey, V., Seneviratne, S. I., and Gudmundsson, L.: GRUN: an observation-based global gridded runoff dataset from 1902 to 2014, *Earth Syst. Sci. Data*, 11, 1655-1674, 10.5194/essd-11-1655-2019, 2019.
- Golaz, J.-C., Caldwell, P. M., Van Roekel, L. P., Petersen, M. R., Tang, Q., Wolfe, J. D., Abeshu, G., Anantharaj, V., Asay-Davis, X. S., Bader, D. C., Baldwin, S. A., Bisht, G., Bogenschütz, P. A., Branstetter, M., Brunke, M. A., Brus, S. R., Burrows, S. M., Cameron-Smith, P. J., Donahue, A. S., Deakin, M., Easter, R. C., Evans, K. J., Feng, Y., Flanner, M., Foucar, J. G., Fyke, J. G., Griffin, B. M., Hannay, C., 470 Harrop, B. E., Hoffman, M. J., Hunke, E. C., Jacob, R. L., Jacobsen, D. W., Jeffery, N., Jones, P. W., Keen, N. D., Klein, S. A., Larson, V. E., Leung, L. R., Li, H.-Y., Lin, W., Lipscomb, W. H., Ma, P.-L., Mahajan, S., Maltrud, M. E., Mamejtanov, A., McClean, J. L., McCoy, R. B., Neale, R. B., Price, S. F., Qian, Y., Rasch, P. J., Reeves Eyre, J. E. J., Riley, W. J., Ringler, T. D., Roberts, A. F., Roesler, E. L., Salinger, A. G., Shaheen, Z., Shi, X., Singh, B., Tang, J., Taylor, M. A., Thornton, P. E., Turner, A. K., Veneziani, M., Wan, H., Wang, H., Wang, S., Williams, D. N., Wolfram, P. J., Worley, P. H., Xie, S., Yang, Y., Yoon, J.-H., Zelinka, M. D., Zender, C. S., Zeng, X., Zhang, C., Zhang, 475 K., Zhang, Y., Zheng, X., Zhou, T., and Zhu, Q.: The DOE E3SM Coupled Model Version 1: Overview and Evaluation at Standard Resolution, *J Adv Model Earth Sy*, 11, 2089-2129, <https://doi.org/10.1029/2018MS001603>, 2019.
- Gudmundsson, L., Do, H. X., Leonard, M., and Westra, S.: The Global Streamflow Indices and Metadata Archive (GSIM) – Part 2: Quality control, time-series indices and homogeneity assessment, *Earth Syst. Sci. Data*, 10, 787-804, 10.5194/essd-10-787-2018, 2018.
- Gudmundsson, L., Boulange, J., Do, H. X., Gosling, S. N., Grillakis, M. G., Koutroulis, A. G., Leonard, M., Liu, J., Schmied, H. M., 480 Papadimitriou, L., Pokhrel, Y., Seneviratne, S. I., Satoh, Y., Thiery, W., Westra, S., Zhang, X., and Zhao, F.: Globally observed trends in mean and extreme river flow attributed to climate change, *Science*, 371, 1159-1162, doi:10.1126/science.aba3996, 2021.
- Harris, I., Jones, P. D., Osborn, T. J., and Lister, D. H.: Updated high-resolution grids of monthly climatic observations—the CRU TS3. 10 Dataset, *Int J Climatol*, 34, 623-642, 2014.
- Hirabayashi, Y., Mahendran, R., Koirala, S., Konoshima, L., Yamazaki, D., Watanabe, S., Kim, H., and Kanae, S.: Global flood risk under 485 climate change, *Nat Clim Change*, 3, 816-821, 10.1038/nclimate1911, 2013.
- Hirpa, F. A., Salamon, P., Beck, H. E., Lorini, V., Alfieri, L., Zsoter, E., and Dadson, S. J.: Calibration of the Global Flood Awareness System (GloFAS) using daily streamflow data, *J Hydrol*, 566, 595-606, 10.1016/j.jhydrol.2018.09.052, 2018.
- Hobeichi, S., Abramowitz, G., Evans, J., and Beck, H. E.: Linear Optimal Runoff Aggregate (LORA): a global gridded synthesis runoff product, *Hydrol. Earth Syst. Sci.*, 23, 851-870, 10.5194/hess-23-851-2019, 2019.
- 490 Hou, Z., Huang, M., Leung, L. R., Lin, G., and Ricciuto, D. M.: Sensitivity of surface flux simulations to hydrologic parameters based on an uncertainty quantification framework applied to the Community Land Model, *Journal of Geophysical Research: Atmospheres*, 117, <https://doi.org/10.1029/2012JD017521>, 2012.
- Huang, M., Hou, Z., Leung, L. R., Ke, Y., Liu, Y., Fang, Z., and Sun, Y.: Uncertainty Analysis of Runoff Simulations and Parameter Identifiability in the Community Land Model: Evidence from MOPEX Basins, *J Hydrometeorol*, 14, 1754-1772, 10.1175/JHM-D-12- 495 0138.1, 2013.
- Ivory, S. J., McGlue, M. M., Spera, S., Silva, A., and Bergier, I.: Vegetation, rainfall, and pulsing hydrology in the Pantanal, the world's largest tropical wetland, *Environ Res Lett*, 14, 124017, 10.1088/1748-9326/ab4ffe, 2019.
- Jardim, P. F., Melo, M. M. M., Ribeiro, L. d. C., Collischonn, W., and Paz, A. R. d.: A Modeling Assessment of Large-Scale Hydrologic Alteration in South American Pantanal Due to Upstream Dam Operation, *Frontiers in Environmental Science*, 8, 10.3389/fenvs.2020.567450, 2020.
- 500 Jiang, L., Westphal Christensen, S., and Bauer-Gottwein, P.: Calibrating 1D hydrodynamic river models in the absence of cross-section geometry using satellite observations of water surface elevation and river width, *Hydrol. Earth Syst. Sci.*, 25, 6359-6379, 10.5194/hess-25-6359-2021, 2021.
- Jung, M., Koirala, S., Weber, U., Ichii, K., Gans, F., Camps-Valls, G., Papale, D., Schwalm, C., Tramontana, G., and Reichstein, M.: The 505 FLUXCOM ensemble of global land-atmosphere energy fluxes, *Scientific data*, 6, 1-14, 2019.
- Kalnay, E., Kanamitsu, M., Kistler, R., Collins, W., Deaven, D., Gandin, L., Iredell, M., Saha, S., White, G., and Woollen, J.: The NCEP/NCAR 40-year reanalysis project, *B Am Meteorol Soc*, 77, 437-472, 1996.
- Knight, R. R., Murphy, J. C., Wolfe, W. J., Saylor, C. F., and Wales, A. K.: Ecological limit functions relating fish community response to hydrologic departures of the ecological flow regime in the Tennessee River basin, United States, *Ecohydrology*, 7, 1262-1280, 510 <https://doi.org/10.1002/eco.1460>, 2014.



- Knutti, R., Sedlacek, J., Sanderson, B. M., Lorenz, R., Fischer, E. M., and Eyring, V.: A climate model projection weighting scheme accounting for performance and interdependence, *Geophys Res Lett*, 44, 1909-1918, 10.1002/2016gl072012, 2017.
- Lehner, B. and Döll, P.: Development and validation of a global database of lakes, reservoirs and wetlands, *J Hydrol*, 296, 1-22, <https://doi.org/10.1016/j.jhydrol.2004.03.028>, 2004.
- 515 Lehner, B., Verdin, K., and Jarvis, A.: New Global Hydrography Derived From Spaceborne Elevation Data, *Eos, Transactions American Geophysical Union*, 89, 93-94, <https://doi.org/10.1029/2008EO100001>, 2008.
- Lehner, F., Wood, A. W., Vano, J. A., Lawrence, D. M., Clark, M. P., and Mankin, J. S.: The potential to reduce uncertainty in regional runoff projections from climate models, *Nat Clim Change*, 9, 926-933, 10.1038/s41558-019-0639-x, 2019.
- 520 Li, H., Wigmosta, M. S., Wu, H., Huang, M., Ke, Y., Coleman, A. M., and Leung, L. R.: A Physically Based Runoff Routing Model for Land Surface and Earth System Models, *J Hydrometeorol*, 14, 808-828, 10.1175/jhm-d-12-015.1, 2013.
- Li, H.-Y., Leung, L. R., Getirana, A., Huang, M., Wu, H., Xu, Y., Guo, J., and Voisin, N.: Evaluating Global Streamflow Simulations by a Physically Based Routing Model Coupled with the Community Land Model, *J Hydrometeorol*, 16, 948-971, 10.1175/JHM-D-14-0079.1, 2015.
- 525 Liang, X., Lettenmaier, D. P., Wood, E. F., and Burges, S. J.: A simple hydrologically based model of land surface water and energy fluxes for general circulation models, *Journal of Geophysical Research: Atmospheres*, 99, 14415-14428, 10.1029/94JD00483, 1994.
- Liao, C. and Zhuang, Q.: Quantifying the Role of Snowmelt in Stream Discharge in an Alaskan Watershed: An Analysis Using a Spatially Distributed Surface Hydrology Model, *Journal of Geophysical Research: Earth Surface*, 122, 2183-2195, <https://doi.org/10.1002/2017JF004214>, 2017.
- 530 Liao, C., Zhou, T., Xu, D., Barnes, R., Bisht, G., Li, H.-Y., Tan, Z., Tesfa, T., Duan, Z., Engwirda, D., and Leung, L. R.: Advances in hexagon mesh-based flow direction modeling, *Adv Water Resour*, 160, 104099, <https://doi.org/10.1016/j.advwatres.2021.104099>, 2022.
- Libonati, R., DaCamara, C. C., Peres, L. F., Sander de Carvalho, L. A., and Garcia, L. C.: Rescue Brazil's burning Pantanal wetlands, 2020.
- Luo, X., Li, H. Y., Leung, L. R., Tesfa, T. K., Getirana, A., Papa, F., and Hess, L. L.: Modeling surface water dynamics in the Amazon Basin using MOSART-Inundation v1.0: impacts of geomorphological parameters and river flow representation, *Geosci. Model Dev.*, 10, 1233-1259, 10.5194/gmd-10-1233-2017, 2017.
- 535 Mao, Y., Zhou, T., Leung, L. R., Tesfa, T. K., Li, H.-Y., Wang, K., Tan, Z., and Getirana, A.: Flood Inundation Generation Mechanisms and Their Changes in 1953–2004 in Global Major River Basins, *Journal of Geophysical Research: Atmospheres*, 124, 11672-11692, 10.1029/2019JD031381, 2019.
- Martens, B., Miralles, D. G., Lievens, H., van der Schalie, R., de Jeu, R. A. M., Fernández-Prieto, D., Beck, H. E., Dorigo, W. A., and Verhoest, N. E. C.: GLEAM v3: satellite-based land evaporation and root-zone soil moisture, *Geosci. Model Dev.*, 10, 1903-1925, 10.5194/gmd-10-1903-2017, 2017.
- 540 Milly, P. C. D., Dunne, K. A., and Vecchia, A. V.: Global pattern of trends in streamflow and water availability in a changing climate, *Nature*, 438, 347-350, 10.1038/nature04312, 2005.
- Milly, P. C. D., Wetherald, R. T., Dunne, K. A., and Delworth, T. L.: Increasing risk of great floods in a changing climate, *Nature*, 415, 514-517, DOI 10.1038/415514a, 2002.
- 545 Niu, G.-Y., Yang, Z.-L., Dickinson, R. E., and Gulden, L. E.: A simple TOPMODEL-based runoff parameterization (SIMTOP) for use in global climate models, *Journal of Geophysical Research: Atmospheres*, 110, <https://doi.org/10.1029/2005JD006111>, 2005.
- Oleson, K., Lawrence, D. M., Bonan, G. B., Drewniak, B., Huang, M., Koven, C. D., Levis, S., Li, F., Riley, W. J., Subin, Z. M., Swenson, S., Thornton, P. E., Bozbiyik, A., Fisher, R., Heald, C. L., Kluzek, E., Lamarque, J.-F., Lawrence, P. J., Leung, L. R., Lipscomb, W., Muszala, S. P., Ricciuto, D. M., Sacks, W. J., Sun, Y., Tang, J., and Yang, Z.-L.: Technical description of version 4.5 of the Community Land Model (CLM), <http://dx.doi.org/10.5065/D6RR1W7M>, 2013.
- 550 Pickens, A. H., Hansen, M. C., Hancher, M., Stehman, S. V., Tyukavina, A., Potapov, P., Marroquin, B., and Sherani, Z.: Mapping and sampling to characterize global inland water dynamics from 1999 to 2018 with full Landsat time-series, *Remote Sens Environ*, 243, 111792, <https://doi.org/10.1016/j.rse.2020.111792>, 2020.
- Qian, Y., Jackson, C., Giorgi, F., Booth, B., Duan, Q., Forest, C., Higdon, D., Hou, Z. J., and Huerta, G.: Uncertainty Quantification in Climate Modeling and Projection, *B Am Meteorol Soc*, 97, 821-824, 10.1175/BAMS-D-15-00297.1, 2016.
- 555 Qian, Y., Wan, H., Yang, B., Golaz, J.-C., Harrop, B., Hou, Z., Larson, V. E., Leung, L. R., Lin, G., Lin, W., Ma, P.-L., Ma, H.-Y., Rasch, P., Singh, B., Wang, H., Xie, S., and Zhang, K.: Parametric Sensitivity and Uncertainty Quantification in the Version 1 of E3SM Atmosphere Model Based on Short Perturbed Parameter Ensemble Simulations, *Journal of Geophysical Research: Atmospheres*, 123, 13,046-013,073, <https://doi.org/10.1029/2018JD028927>, 2018.
- 560 Ricciuto, D., Sargsyan, K., and Thornton, P.: The Impact of Parametric Uncertainties on Biogeochemistry in the E3SM Land Model, *J Adv Model Earth Sy*, 10, 297-319, 10.1002/2017ms000962, 2018.
- Schewe, J., Heinke, J., Gerten, D., Haddeland, I., Arnell, N. W., Clark, D. B., Dankers, R., Eisner, S., Fekete, B. M., Colón-González, F. J., Gosling, S. N., Kim, H., Liu, X., Masaki, Y., Portmann, F. T., Satoh, Y., Stacke, T., Tang, Q., Wada, Y., Wisser, D., Albrecht, T., Frieler, K., Piontek, F., Warszawski, L., and Kabat, P.: Multimodel assessment of water scarcity under climate change, *Proceedings of the National Academy of Sciences*, 111, 3245-3250, 10.1073/pnas.1222460110, 2014.
- 565



- Schrapffer, A., Sörensson, A., Polcher, J., and Fita, L.: Benefits of representing floodplains in a Land Surface Model: Pantanal simulated with ORCHIDEE CMIP6 version, *Clim Dynam*, 55, 1303-1323, 10.1007/s00382-020-05324-0, 2020.
- Sen, P. K.: Estimates of the Regression Coefficient Based on Kendall's Tau, *J Am Stat Assoc*, 63, 1379-1389, 10.1080/01621459.1968.10480934, 1968.
- 570 Shaad, K.: Evolution of river-routing schemes in macro-scale models and their potential for watershed management, *Hydrological Sciences Journal*, 63, 1062-1077, 10.1080/02626667.2018.1473871, 2018.
- Shen, H., Tolson, B. A., and Mai, J.: Time to Update the Split-Sample Approach in Hydrological Model Calibration, *Water Resour Res*, 58, e2021WR031523, <https://doi.org/10.1029/2021WR031523>, 2022.
- 575 Sheng, M., Lei, H., Jiao, Y., and Yang, D.: Evaluation of the Runoff and River Routing Schemes in the Community Land Model of the Yellow River Basin, *J Adv Model Earth Sy*, 9, 2993-3018, <https://doi.org/10.1002/2017MS001026>, 2017.
- Slater, J. L. and Villarini, G.: Evaluating the Drivers of Seasonal Streamflow in the U.S. Midwest, *Water*, 9, 10.3390/w9090695, 2017.
- Smith, R. L., Tebaldi, C., Nychka, D., and Mearns, L. O.: Bayesian Modeling of Uncertainty in Ensembles of Climate Models, *J Am Stat Assoc*, 104, 97-116, 2009.
- 580 Tebaldi, C., Smith, R. L., Nychka, D., and Mearns, L. O.: Quantifying uncertainty in projections of regional climate change: A Bayesian approach to the analysis of multimodel ensembles, *J Climate*, 18, 1524-1540, Doi 10.1175/Jcli3363.1, 2005.
- Troy, T. J., Wood, E. F., and Sheffield, J.: An efficient calibration method for continental-scale land surface modeling, *Water Resour Res*, 44, <https://doi.org/10.1029/2007WR006513>, 2008.
- Vivoni, E., Entekhabi, D., Bras, R., and Ivanov, V.: Controls on runoff generation and scale-dependence in a distributed hydrologic model, *Hydrol Earth Syst Sc*, 11, 1683-1701, 2007.
- 585 Voisin, N., Li, H., Ward, D., Huang, M., Wigmosta, M., and Leung, L. R.: On an improved sub-regional water resources management representation for integration into earth system models, *Hydrol. Earth Syst. Sci.*, 17, 3605-3622, 10.5194/hess-17-3605-2013, 2013.
- Wu, H., Kimball, J. S., Mantua, N., and Stanford, J.: Automated upscaling of river networks for macroscale hydrological modeling, *Water Resour Res*, 47, <https://doi.org/10.1029/2009WR008871>, 2011.
- Xu, D.: donghuix/E3SM: New wetland inundation scheme, 10.5281/zenodo.6982264, 2022.
- 590 Xu, D.: Scripts and Data for "Disentangling the Hydrological and Hydraulic Controls on Streamflow Variability in E3SM V2 – A Case Study in the Pantanal Region", 10.5281/zenodo.8290236, 2023.
- Xu, D., Ivanov, V. Y., Agee, E., and Wang, J.: Energy Surplus and an Atmosphere-Land-Surface "Tug of War" Control Future Evapotranspiration, *Geophys Res Lett*, 50, e2022GL102677, <https://doi.org/10.1029/2022GL102677>, 2023a.
- Xu, D., Ivanov, V. Y., Kim, J., and Fatichi, S.: On the use of observations in assessment of multi-model climate ensemble, *Stochastic Environmental Research and Risk Assessment*, 33, 1923-1937, 10.1007/s00477-018-1621-2, 2019.
- 595 Xu, D., Ivanov, V. Y., Li, X., and Troy, T. J.: Peak Runoff Timing is Linked to Global Warming Trajectories, *Earth's Future*, n/a, e2021EF002083, <https://doi.org/10.1029/2021EF002083>, 2021.
- Xu, D., Bisht, G., Sargsyan, K., Liao, C., and Leung, L. R.: Using a surrogate-assisted Bayesian framework to calibrate the runoff-generation scheme in the Energy Exascale Earth System Model (E3SM) v1, *Geosci. Model Dev.*, 15, 5021-5043, 10.5194/gmd-15-5021-2022, 2022a.
- 600 Xu, D., Bisht, G., Zhou, T., Leung, L. R., and Pan, M.: Development of Land-River Two-Way Hydrologic Coupling for Floodplain Inundation in the Energy Exascale Earth System Model, *J Adv Model Earth Sy*, 14, e2021MS002772, <https://doi.org/10.1029/2021MS002772>, 2022b.
- Xu, D., Bisht, G., Tan, Z., Sinha, E., Di Vittorio, A., Zhou, T., Ivanov, V., and Leung, L.: Climate change reduces wetland size and shifts its seasonal regime in North America, 2023b.
- 605 Yamazaki, D., Oki, T., and Kanae, S.: Deriving a global river network map and its sub-grid topographic characteristics from a fine-resolution flow direction map, *Hydrol. Earth Syst. Sci.*, 13, 2241-2251, 10.5194/hess-13-2241-2009, 2009.
- Yamazaki, D., Kanae, S., Kim, H., and Oki, T.: A physically based description of floodplain inundation dynamics in a global river routing model, *Water Resour Res*, 47, 10.1029/2010WR009726, 2011.
- 610 Yang, H., Zhou, F., Piao, S. L., Huang, M. T., Chen, A. P., Ciais, P., Li, Y., Lian, X., Peng, S. S., and Zeng, Z. Z.: Regional patterns of future runoff changes from Earth system models constrained by observation, *Geophys Res Lett*, 44, 5540-5549, 10.1002/2017gl073454, 2017.
- Yang, Y., Pan, M., Beck, H. E., Fisher, C. K., Beighley, R. E., Kao, S. C., Hong, Y., and Wood, E. F.: In quest of calibration density and consistency in hydrologic modeling: distributed parameter calibration against streamflow characteristics, *Water Resour Res*, 55, 7784-7803, 2019.
- 615 Yang, Y., Pan, M., Lin, P., Beck, H. E., Zeng, Z., Yamazaki, D., David, C. d. H., Lu, H., Yang, K., Hong, Y., and Wood, E. F.: Global Reach-level 3-hourly River Flood Reanalysis (1980-2019), *B Am Meteorol Soc*, 1-49, 10.1175/BAMS-D-20-0057.1, 2021.
- Zhang, Y., Zheng, H., Chiew, F. H. S., Arancibia, J. P. a., and Zhou, X.: Evaluating Regional and Global Hydrological Models against Streamflow and Evapotranspiration Measurements, *J Hydrometeorol*, 17, 995-1010, 10.1175/JHM-D-15-0107.1, 2016.

<https://doi.org/10.5194/egusphere-2023-1879>

Preprint. Discussion started: 30 August 2023

© Author(s) 2023. CC BY 4.0 License.



620 Zhou, T., Leung, L. R., Leng, G., Voisin, N., Li, H.-Y., Craig, A. P., Tesfa, T., and Mao, Y.: Global Irrigation Characteristics and Effects Simulated by Fully Coupled Land Surface, River, and Water Management Models in E3SM, *J Adv Model Earth Sy*, 12, e2020MS002069, <https://doi.org/10.1029/2020MS002069>, 2020.